Databases of flow and near pressure field signals obtained for compressible round jets using large-eddy simulations

Christophe Bogey[1]

Univ Lyon, Ecole Centrale de Lyon, INSA Lyon, Université Claude Bernard Lyon I, CNRS, Laboratoire de Mécanique des Fluides et d'Acoustique, UMR 5509, F-69134, Ecully, France

Email: christophe.bogey@ec-lyon.fr

(updated on January 13, 2022)

Databases of signals obtained in the flow and near pressure fields of compressible turbulent round jets computed by highly-resolved large-eddy simulations (LES) using cylindrical coordinates (r, θ, z) have been built up. They are available upon request by email. A brief description of the jet exit conditions, grid parameters and recorded signals is given below.

1 Jet exit conditions

1.1 Reference, isothermal jets at a Mach number of 0.9 and at low and high Reynolds numbers

At the beginning, two isothermal jets at a Mach number of 0.9 at diameter-based Reynolds numbers $\mathrm{Re}_D = 3125$ and $\mathrm{Re}_D = 10^5$ [1], represented by a red diamond and a red bullet in figure 1, have been simulated. Their initial conditions are given in table 1. The parameters of the simulations and flow and noise properties of the jets are presented in recent papers [2, 3, 4, 5, 6]. More results can be found in references [7, 8, 9]. The grid used are referred to as CGz75a and FGz40, see in section 3. The set of files recorded are D2 and D0, see in section 4. The recording times Tu_j/r_0 are equal to or greater than $3,625$. The simulation of M09Re1e5TaLd0150v9 is ongoing.

jet	M	Re_D	T_j/T_a	BL	δ_{BL}/r_0	u'_e/u_j	grid	n_θ	Tu_j/r_0	data
M09Re3125TaLd0420v1	0.9	3,125	1	L	0.42	1%	CGz75	512	5,000	D2
M09Re1e5TaLd0150v9	0.9	100,000	1	L	0.15	9%	FGz40	1,024	3,625	D0

Table 1: Mach and Reynolds numbers M and Re_D, jet temperature T_j, shape (L: laminar Blasius, T: transitional or turbulent) and thickness δ_{BL} of the boundary-layer profile imposed at the pipe nozzle inlet, peak turbulence intensity u'_e/u_j at the nozzle exit, grid used, number of points n_θ in the azimuthal direction , simulation time T after the transient period and recording files.

1.2 Low-Reynolds-number isothermal jets

On the basis of the simulation of the jet M09Re3125TaLd0420v1 at M = 0.9 and $\mathrm{Re}_D = 3,125$, isothermal jets also at $\mathrm{Re}_D = 3125$ but at M = 0.3, 0.45, 0.6, 1.3 and 2, with peak turbulence

[1]CNRS Research Scientist, ORCID iD: https://orcid.org/0000-0003-3243-747X

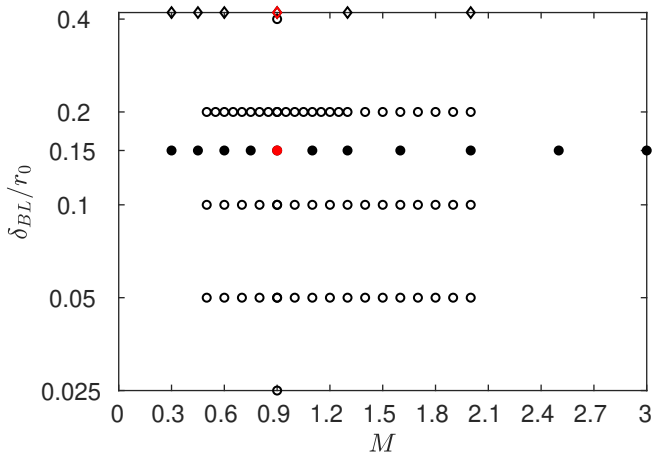

Figure 1: Jets at $\mathrm{Re}_D = 10^5$ with • tripped and ○ untripped boundary layers, and ◇ at $\mathrm{Re}_D = 3125$: Mach number M and thickness δ_{BL} of the Blasius profiles at the pipe-nozzle inlet; ◇ M09Re3125TaLd0420v1 and • M09Re1e5TaLd0150v9.

intensity $u'_e/u_j \simeq 0.01$ at the nozzle exit, have been computed. They are collected in table 2, and represented by diamonds in figure 1. The simulations are ongoing for M = 0.3, 0.45 and 2.

jet	M	Re_D	T_j/T_a	BL	δ_{BL}/r_0	u'_e/u_j	grid	n_θ	Tu_j/r_0	data
M03Re3125TaLd0420v1	0.3	3,125	1	L	0.42	1%	CGz75a	512	1,000	D2
M045Re3125TaLd0420v1	0.45	3,125	1	L	0.42	1%	CGz75a	512	1,500	D2
M06Re3125TaLd0420v1	0.6	3,125	1	L	0.42	1%	CGz75a	512	4,000	D2
M09Re3125TaLd0420v1	0.9	3,125	1	L	0.42	1%	CGz75a	512	5,000	D2
M13Re3125TaLd0420v1	1.3	3,125	1	L	0.42	1%	CGz75b	512	4,000	D2
M2Re3125TaLd0420v2_5	2	3,125	1	L	0.42	2.5%	CGz90	512	3,000	D2

Table 2: See caption of table 1.

1.3 High-Reynolds-number isothermal jets with untripped boundary-layers

Isothermal jets at $\mathrm{Re}_D = 10^5$ with untripped boundary-layers have been considered in order to investigate the flow and sound fields of initially fully laminar jets. They are represented by circles in figure 1. The cost of the simulations of such jets is also much cheaper than that of jets with tripped boundary-layers.

1.3.1 Isothermal jets at a Mach number of 0.9

Isothermal jets at M = 0.9 with untripped boundary-layers of different thickness [10] have been computed. They are defined in table 3. Some results of the simulations are presented in recent papers [2, 4, 5, 6].

1.3.2 Isothermal jets at Mach numbers between 0.5 and 2

Isothermal jets with untripped boundary-layers of different thickness at Mach numbers varying between 0.5 and 2 in increments of 0.05 or 0.1 have been computed. They are defined in table 4. Some results of the simulations are presented in recent papers [4, 5].

jet	M	Re_D	T_j/T_a	L	δ_{BL}/r_0	u'_e/u_j	grid	n_θ	Tu_j/r_0	data
M09Re1e5TaLd0400v0	0.9	100,000	1	L	0.4	0%	FGz40	256	500	D1
M09Re1e5TaLd0200v0	0.9	100,000	1	L	0.2	0%	FGz40	256	3,000	D1
M09Re1e5TaLd0100v0	0.9	100,000	1	L	0.1	0%	FGz40	512	1,000	D1
M09Re1e5TaLd0050v0	0.9	100,000	1	L	0.05	0%	FGz40	512	1,000	D1
M09Re1e5TaLd0025v0	0.9	100,000	1	L	0.025	0%	FGz40	512	2,000	D1

Table 3: See caption of table 1.

jet	M	Re_D	T_j/T_a	L	δ_{BL}/r_0	u'_e/u_j	grid	n_θ	Tu_j/r_0	data
MxxxRe1e5TaLd0200v0	$0.5 \to 2$	100,000	1	L	0.2	0%	FGz40	256	500	D3
MxxxRe1e5TaLd0100v0	$0.5 \to 2$	100,000	1	L	0.1	0%	FGz40	256	500	D3
MxxxRe1e5TaLd0050v0	$0.5 \to 2$	100,000	1	L	0.05	0%	FGz40	256	500	D3

Table 4: See caption of table 1.

1.4 High-Reynolds-number isothermal jets with tripped boundary-layers

Isothermal jets at $\mathrm{Re}_D = 10^5$ with tripped boundary-layers have been considered in order to investigate the flow and sound fields of initially highly disturbed jets. They are characterized by peak turbulence intensity u'_e/u_j typically of 9% at the nozzle exit.

1.4.1 Isothermal jets with nozzle-exit turbulence levels between 0 and 15%

Isothermal jets at M = 0.9 and $\mathrm{Re}_D = 10^5$ with peak turbulence intensity at the nozzle exit $u'_e/u_j = 0$, 3%, 6%, 9%, 12% and 15% [1, 11, 12] have been computed. They are defined in table 5.

jet	M	Re_D	T_j/T_a	BL	δ_{BL}/r_0	u'_e/u_j	grid	n_θ	Tu_j/r_0	data
M09Re1e5TaLd0150v0	0.9	100,000	1	L	0.15	0%	FGz40	512	500	D1
M09Re1e5TaLd0150v3	0.9	100,000	1	L	0.15	3%	FGz40	1,024	500	D1
M09Re1e5TaLd0150v6	0.9	100,000	1	L	0.15	6%	FGz40	1,024	500	D1
M09Re1e5TaLd0150v9	0.9	100,000	1	L	0.15	9%	FGz40	1,024	3,625	D0
M09Re1e5TaLd0150v12	0.9	100,000	1	L	0.15	12%	FGz40	1,024	500	D1
M09Re1e5TaLd0150v15	0.9	100,000	1	L	0.15	15%	FGz40	1,024	500	D1

Table 5: See caption of table 1.

1.4.2 Isothermal jets at Reynolds numbers between 12,500 and 400,000

Isothermal jets with highly disturbed boundary layers at M = 0.9 and Re_D varying between 12,500 and 400,000 [13] have been computed. They are presented in table 6.

1.4.3 Isothermal jets with different boundary-layer thicknesses

Isothermal jets at M = 0.9 with highly disturbed boundary layers of different thickness [14] have been computed. They are reported in table 7. Results are available in [15].

jet	M	Re_D	T_j/T_a	BL	δ_{BL}/r_0	u'_e/u_j	grid	n_θ	Tu_j/r_0	data
M09Re1_25e4TaLd0150v7_5	0.9	12,500	1	L	0.15	7.5%	FGz40	1,024	500	D1
M09Re2_5e4TaLd0150v9	0.9	25,000	1	L	0.15	9%	FGz40	1,024	500	D1
M09Re5e4TaLd0150v9	0.9	50,000	1	L	0.15	9%	FGz40	1,024	500	D1
M09Re1e5TaLd0150v9	0.9	100,000	1	L	0.15	9%	FGz40	1,024	3,000	D0
M09Re2e5TaLd0150v9	0.9	200,000	1	L	0.15	9%	FGz40	1,024	500	D1
M09Re4e5TaLd0150v9	0.9	400,000	1	L	0.15	9%	FGz40	1,024	500	D1

Table 6: See caption of table 1.

jet	M	Re_D	T_j/T_a	L	δ_{BL}/r_0	u'_e/u_j	grid	n_θ	Tu_j/r_0	data
M09Re5e4TaLd0150v9	0.9	50,000	1	L	0.15	9%	FGz40	1,024	500	D1
M09Re5e4TaLd0090v9	0.9	50,000	1	L	0.09	9%	FGz40	1,024	500	D1
M09Re5e4TaLd0250v9	0.9	50,000	1	L	0.25	9%	FGz40	1,024	500	D1
M09Re5e4TaLd0420v9	0.9	50,000	1	L	0.42	9%	FGz40	1,024	500	D1
M09Re8_3e4TaLd0250v9	0.9	83,333	1	L	0.09	9%	FGz40	1,024	500	D1
M09Re3e4TaLd0250v9	0.9	30,000	1	L	0.25	9%	FGz40	1,024	500	D1
M09Re1_8e4TaLd0250v9	0.9	18,000	1	L	0.42	9%	FGz40	1,024	500	D1

Table 7: See caption of table 1.

1.4.4 Isothermal jets at Mach numbers between 0.3 and 3

On the basis of the simulation of the jet M09Re1e5TaLd0150v9 at M = 0.9 and $\mathrm{Re}_D = 100,000$, isothermal jets also at $\mathrm{Re}_D = 100,000$ but at M = 0.3, 0.45, 0.6, 0.75, 1.1, 1.3, 1.6, 2, 2.5 and 3 have been computed. They are collected in table 8, and are represented by bullets in figure 1. The parameters of the simulations and the flow and noise properties of the jets at M = 0.6, 0.75, 1.1, 1.3 and 2 are presented in recent papers [4, 5, 6]. The simulations are ongoing for all jets.

jet	M	Re_D	T_j/T_a	BL	δ_{BL}/r_0	u'_e/u_j	grid	n_θ	Tu_j/r_0	data
M03Re1e5TaLd0150v9	0.3	100,000	1	L	0.15	9%	FGz40	1,024	500	D1
M045Re1e5TaLd0150v9	0.45	100,000	1	L	0.15	9%	FGz40	1,024	800	D1
M06Re1e5TaLd0150v9	0.6	100,000	1	L	0.15	9%	FGz40	1,024	2,000	D1
M075Re1e5TaLd0150v9	0.75	100,000	1	L	0.15	9%	FGz40	1,024	2,000	D1
M09Re1e5TaLd0150v9	0.9	100,000	1	L	0.15	9%	FGz40	1,024	3,625	D0
M11Re1e5TaLd0150v9	1.1	100,000	1	L	0.15	9%	FGz40	1,024	2,000	D1
M13Re1e5TaLd0150v9	1.3	100,000	1	L	0.15	9%	FGz50	1,024	2,000	D1
M16Re1e5TaLd0150v9	1.6	100,000	1	L	0.15	9%	FGz50	1,024	600	D1
M2Re1e5TaLd0150v9	2	100,000	1	L	0.15	9%	FGz60	1,024	2,000	D1
M25Re1e5TaLd0150v9	2.5	100,000	1	L	0.15	9%	FGz60	1,024	400	D1
M3Re1e5TaLd0150v9	3	100,000	1	L	0.15	9%	FGz70	1,024	600	D1

Table 8: See caption of table 1.

1.4.5 Isothermal jets with non-laminar boundary-layer shape

Isothermal jets at M = 0.9 and $\mathrm{Re}_D = 50,000$ with highly disturbed boundary layers of different shapes [16] (laminar L and non-laminar T1, T2 and T3) have been computed. They are defined in table 9. The parameters of the simulations and the flow and noise properties of the jets are presented

in recent papers [17, 15].

jet	M	Re_D	T_j/T_a	BL	δ_{BL}/r_0	u'_e/u_j	grid	n_θ	Tu_j/r_0	data
M09Re5e4TaLd0250v0	0.9	50,000	1	L	0.25	0%	FGz40	1,024	500	D1
M09Re5e4TaT1d0250v0	0.9	50,000	1	T1	0.25	0%	FGz40	1,024	500	D1
M09Re5e4TaT2d0250v0	0.9	50,000	1	T2	0.25	0%	FGz40	1,024	500	D1
M09Re5e4TaT3d0250v0	0.9	50,000	1	T3	0.25	0%	FGz40	1,024	500	D1
M09Re5e4TaLd0250v6	0.9	50,000	1	L	0.25	6%	FGz40	1,024	500	D1
M09Re5e4TaT1d0250v6	0.9	50,000	1	T1	0.25	6%	FGz40	1,024	500	D1
M09Re5e4TaT2d0250v6	0.9	50,000	1	T2	0.25	6%	FGz40	1,024	500	D1

Table 9: See caption of table 1.

1.4.6 Hot jets at a Mach number of 0.9

Hot jets at M = 0.9 and Re_D between 25,000 and 200,000 with highly disturbed boundary layers [18, 19] have been computed. Their nozzle-exit static temperatures are $T_j = 1.5T_a$ or $T_j = 2.25T_a$. They are defined in table 10. The simulations are ongoing for M09Re1e5Ta1_5Ld0150v9 and M09Re1e5Ta2_25Ld0150v9.

jet	M	Re_D	T_j/T_a	BL	δ_{BL}/r_0	u'_e/u_j	grid	n_θ	Tu_j/r_0	data
M09Re1e5TaLd0150v9	0.9	100,000	1	L	0.15	9%	FGz40	1,024	3,625	D0
M09Re5e4Ta1_5Ld0150v9	0.9	50,000	1.5	L	0.15	9%	FGz40	1,024	500	D1
M09Re1e5Ta1_5Ld0150v9	0.9	100,000	1.5	L	0.15	9%	FGz40	1,024	1,800	D1
M09Re2e5Ta1_5Ld0150v9	0.9	200,000	1.5	L	0.15	9%	FGz40	1,024	500	D1
M09Re2_5e4Ta2_25Ld0150v9	0.9	25,000	2.25	L	0.15	9%	FGz40	1,024	500	D1
M09Re1e5Ta2_25Ld0150v9	0.9	100,000	2.25	L	0.15	9%	FGz40	1,024	1,800	D1

Table 10: See caption of table 1.

1.4.7 Hot jets at Mach numbers between 0.3 and 1.3

Finally, hot jets at $\mathrm{Re}_D = 100,000$ and at M = 0.45, 0.6, 0.75, 1.1 and 1.3 with highly disturbed boundary layers [18, 19] have been computed. Their nozzle-exit static temperatures are $T_j = 1.5T_a$ or $T_j = 2.25T_a$. They are defined in table 11. The simulations are all ongoing.

2 Grid parameters

Some characteristics of the mesh grids used for the simulations in the radial and axial directions are provided in table 12. The CG (coarse) and FG (fine) grids are employed for the jets at $\mathrm{Re}_D = 3,125$ and $\mathrm{Re}_D \geq 12,500$, respectively; z$XX$ indicates that the grid extends down to $z = L_z = XXr_0$ in the axial direction, excluding the outflow sponge zone. The grids are detailed in recent papers [2, 3, 4, 5]. The numbers of points n_θ in the azimuthal direction (256, 512 or 1024) in the different simulations are given in tables 1-10. For illustration purposes, the variations of the radial and axial mesh spacings in FGz40, FGz50 and FGz60 are shown in figure 2.

jet	M	Re_D	T_j/T_a	BL	δ_{BL}/r_0	u'_e/u_j	grid	n_θ	Tu_j/r_0	data
M045Re1e5Ta1_5Ld0150v9	0.45	100,000	1.5	L	0.15	9%	FGz40	1,024	400	D1
M06Re1e5Ta1_5Ld0150v9	0.6	100,000	1.5	L	0.15	9%	FGz40	1,024	400	D1
M075Re1e5Ta1_5Ld0150v9	0.75	100,000	1.5	L	0.15	9%	FGz40	1,024	400	D1
M09Re1e5Ta1_5Ld0150v9	0.9	100,000	1.5	L	0.15	9%	FGz40	1,024	1,800	D1
M11Re1e5Ta1_5Ld0150v9	1.1	100,000	1.5	L	0.15	9%	FGz40	1,024	400	D1
M13Re1e5Ta1_5Ld0150v9	1.3	100,000	1.5	L	0.15	9%	FGz40	1,024	300	D1
M06Re1e5Ta2_25Ld0150v9	0.6	100,000	2.25	L	0.15	9%	FGz40	1,024	50	D1
M075Re1e5Ta2_25Ld0150v9	0.75	100,000	2.25	L	0.15	9%	FGz40	1,024	400	D1
M09Re1e5Ta2_25Ld0150v9	0.9	100,000	2.25	L	0.15	9%	FGz40	1,024	1,800	D1
M11Re1e5Ta2_25Ld0150v9	1.1	100,000	2.25	L	0.15	9%	FGz40	1,024	400	D1
M13Re1e5Ta2_25Ld0150v9	1.3	100,000	2.25	L	0.15	9%	FGz40	1,024	200	D1

Table 11: See caption of table 1.

					$\Delta r/r_0$ (%) at			$\Delta z/r_0$ (%) at		
grid	n_r	n_z	L_r	L_z	$r=0$	$r=r_0$	$r=L_r$	$z=0$	$z=15r_0$	$z=L_z$
CGz75a	427	2458	$25r_0$	$75r_0$	2.48	0.72	14.94	1.45	2.49	6.25
CGz75b	479	2458	$25r_0$	$75r_0$	2.48	0.72	10.03	1.45	2.49	6.25
CGz90	479	3058	$25r_0$	$90r_0$	2.48	0.72	10.03	1.45	2.49	6.25
FGz40	504	2085	$15r_0$	$40r_0$	1.41	0.36	7.55	0.72	2.30	4.88
FGz50	572	2412	$15r_0$	$50r_0$	1.41	0.36	5.03	0.72	2.12	5.31
FGz60	572	2947	$15r_0$	$60r_0$	1.41	0.36	5.03	0.72	1.82	4.95
FGz70	626	3822	$15r_0$	$70r_0$	1.41	0.36	4.02	0.72	1.47	4

Table 12: Numbers of points n_r and n_z and extents of the physical domain L_r and L_z in the radial and axial directions, and mesh spacings Δr and Δz at different positions.

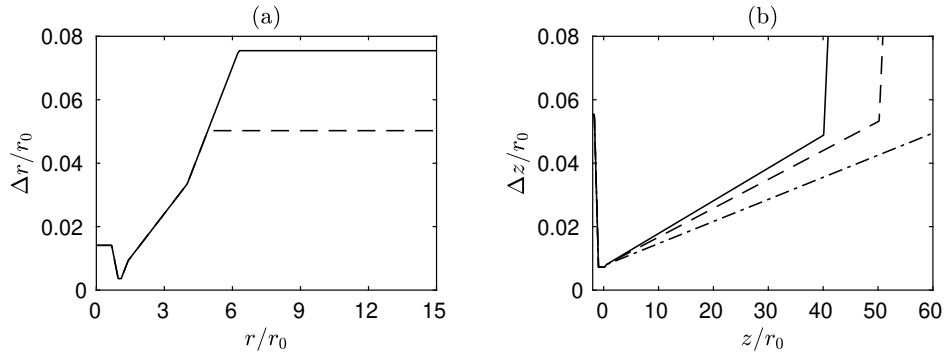

Figure 2: Variations (a) of radial mesh spacing Δr for ——— FGz40 and − − − FGz50 and FGz60 and (b) of axial mesh spacing Δz for ——— FGz40, − − − FGz50 and − · − · FGz60.

3 Database parameters

The recording files are defined in table 13: 3-D fields are stored in the 3Dxxx files, 2-D fields at constant radial, azimuthal and axial positions are stored in the Rxx, Txx and Zxx files, respectively. The maximum Strouhal number allowed by the sampling frequency is equal to 32 for T_{HF} and to 6.4 or 12.8 in the other cases.

files	St_D	z	r	θ	variables
$3Daero$	6.4	$0 \to 30r_0$ every $2\Delta z$	$0 \to 6r_0$ every $2\Delta r$	$0 \to 2\pi - 2\pi/512$ every $2\pi/512$	ρ, u_i, p
$3Dac$	6.4	$0 \to L_z$ every $2\Delta z$	L_r	$0 \to 2\pi - 2\pi/512$ every $2\pi/512$	p
	6.4	$0 \to L_z$ every $2\Delta z$	$0 \to L_r$ every Δr	$0 \to 3\pi/2$ every $\pi/2$	p
	6.4	$0 \to L_z$ every $10r_0$	$0 \to L_r$ every Δr	$0 \to 2\pi - 2\pi/512$ every $2\pi/512$	p
R_0	12.8	$-1.25r_0 \to L_z$ every $2\Delta z$	0	$0 \to 2\pi - 2\pi/256$ every $2\pi/256$	$\rho, u_i, p, \lvert\omega\rvert, \Theta$
R_1	12.8	$-1.25r_0 \to L_z$ every $2\Delta z$	r_0	$0 \to 2\pi - 2\pi/256$ every $2\pi/256$	$\rho, u_i, p, \lvert\omega\rvert, \Theta$
R_{WP}	12.8	$-1.25r_0 \to L_z$ every $2\Delta z$	$1.4r_0$ at $z = 0$ 8^o cone angle	$0 \to 2\pi - 2\pi/256$ every $2\pi/256$	$\rho, u_i, p, \lvert\omega\rvert, \Theta$
R_{NF}	12.8	$-1.25r_0 \to L_z$ every $2\Delta z$	L_r	$0 \to 2\pi - 2\pi/256$ every $2\pi/256$	ρ, u_i, p
T_{axi}	6.4	$-1.25r_0 \to L_z$ every Δz	$0 \to L_r$ every Δr		Fourier coef $n_{\theta=0}$ for ρ, u_i, p
T_{0-270}	6.4	$-1.25r_0 \to L_z$ every Δz	$0 \to L_r$ every Δr	$0 \to 3\pi/2$ every $\pi/2$	$\rho, u_i, p, \partial u_i/\partial\theta$
T_{45-315}	6.4	$-1.25r_0 \to L_z$ every Δz	$0 \to L_r$ every Δr	$\pi/4 \to 13\pi/4$ every $\pi/2$	$\rho, u_i, p, \partial u_i/\partial\theta$
$T_{n_\theta=0-4}$	6.4	$0 \to L_z$ every $2\Delta z$	$0 \to L_r$ every $2\Delta r$		Fourier coef $n_{\theta=0\to4}$ for $\rho, u_i, p, \lvert\omega\rvert, \Theta$
$T_{n_\theta=5-8}$	6.4	$0 \to L_z$ every $2\Delta z$	$0 \to L_r$ every $2\Delta r$		Fourier coef $n_{\theta=5\to8}$ for $\rho, u_i, p, \lvert\omega\rvert, \Theta$
T_{HF}	32	$0 \to 20r_0$ every $2\Delta z$	$0 \to 3.5r_0$ every $2\Delta r$	0	ρ, u_i, p
$Z_{0/start/end}$	12.8	$-1.25r_0, 0, L_z$	$0 \to L_r$ every Δr	$0 \to 2\pi - 2\pi/256$ every $2\pi/256$	ρ, u_i, p
Z_{5-35}	6.4	$5r_0 \to 35r_0$ every $5r_0$	$0 \to L_r$ every $2\Delta r$	$0 \to 2\pi - 2\pi/256$ every $2\pi/256$	ρ, u_i, p

Table 13: Recording files: Strouhal number given by the sampling frequency, recording positions, and variables recorded (density ρ, velocity components $u_i = (u_r, u_t, u_z)$, pressure p, vorticity norm $|\omega|$, dilatation Θ).

The set of files recorded in each simulation, referred to as D0, D1, D2 and D3 in tables 1-10, are defined in table 14. For storage issues, all the files are saved (case D0) only for the reference, isothermal tripped jet at Mach 0.9 and Reynolds 100,000 (M09Re1e5TaLd0150v9). For most other jets at high Reynolds numbers, the 3-D fields and the 2-D fields at $\theta = \pi/4 \to 13\pi/4$ every $\pi/2$ are

not stored (case D1). For the jets at Reynolds 3,125, in addition, the Fourier coefficients for $n_{\theta=5-8}$ are not recorded (case D2). Finally, case D3 applies to the untripped jets at M $\neq$ 0.9.

jets	case	files recorded
M09Re1e5TaLd0150v9	D0	all files
most jets at $\mathrm{Re}_D \geq 12,500$	D1	all files except for $3Daero$, $3Dac$ and T_{45-315}
jets at $\mathrm{Re}_D = 3,125$	D2	all files except for $3Daero$, $3Dac$, T_{45-315}, $T_{n_\theta=5-8}$ and T_{HF}
untripped jets at M $\neq$ 0.9	D3	all files except for $3Daero$, $3Dac$, T_{45-315}, $T_{n_\theta=2-8}$, T_{HF} and Z_{5-35}

Table 14: Set of files recorded in each simulation.

References

[1] Bogey, C., Marsden, O., and Bailly, C., "Large-Eddy Simulation of the flow and acoustic fields of a Reynolds number 10^5 subsonic jet with tripped exit boundary layers," *Phys. Fluids*, Vol. 23, No. 3, 2011, pp. 035104.

[2] Bogey, C., "Grid sensitivity of flow field and noise of high-Reynolds-number jets computed by large-eddy simulation," *Int. J. Aeroacoust.*, Vol. 17, No. 4-5, 2018, pp. 399–424.

[3] Bogey, C., "Two-dimensional features of correlations in the flow and near pressure fields of Mach number 0.9 jets," Tech. Rep. 2019-0806, AIAA Paper, 2019.

[4] Bogey, C., "Acoustic tones in the near-nozzle region of jets: characteristics and variations between Mach numbers 0.5 and 2," *J. Fluid Mech.*, Vol. 921, 2021, pp. A3.

[5] Bogey, C., "Acoustic tones in the near-nozzle region of jets: coupling with initial shear-layer instability waves," *J. Fluid Mech.*, , No. submitted, 2022.

[6] Bogey, C., "Tones in the acoustic far field of jets in the upstream direction," *AIAA J.*, , No. to appear, 2022.

[7] Camussi, R. and Bogey, C., "Intermittent statistics of the 0-mode pressure fluctuations in the near field of Mach 0.9 circular jets at low and high Reynolds numbers," *Theor. Comput. Fluid Dyn.*, Vol. 35, No. 2, 2021, pp. 229–247.

[8] Micci, G., Camussi, R., Meloni, S., and Bogey, C., "Intermittency and stochastic modelling of low and high Reynolds number compressible jets," *AIAA J.*, , No. to appear, 2022.

[9] Adam, A., Papamoschou, D., and Bogey, C., "Imprint of vortical structures on the near-field pressure of a turbulent jet," *AIAA J.*, , No. to appear, 2022.

[10] Bogey, C. and Bailly, C., "Influence of nozzle-exit boundary-layer conditions on the flow and acoustic fields of initially laminar jets," *J. Fluid Mech.*, Vol. 663, 2010, pp. 507–539.

[11] Bogey, C., Marsden, O., and Bailly, C., "On the spectra of nozzle-exit velocity disturbances in initially nominally turbulent, transitional jets," *Phys. Fluids*, Vol. 23, No. 9, 2011, pp. 091702.

[12] Bogey, C., Marsden, O., and Bailly, C., "Influence of initial turbulence level on the flow and sound fields of a subsonic jet at a diameter-based Reynolds number of 10^5," *J. Fluid Mech.*, Vol. 701, 2012, pp. 352–385.

[13] Bogey, C., Marsden, O., and Bailly, C., "Effects of moderate Reynolds numbers on subsonic round jets with highly disturbed nozzle-exit boundary layers," *Phys. Fluids*, Vol. 24, No. 10, 2012, pp. 105107.

[14] Bogey, C. and Marsden, O., "Identification of the effects of the nozzle-exit boundary-layer thickness and its corresponding Reynolds number in initially highly disturbed subsonic jets," *Phys. Fluids*, Vol. 25, No. 5, 2013, pp. 055106.

[15] Bogey, C., "Generation of excess noise by jets with highly disturbed laminar boundary-layer profiles," *AIAA J.*, Vol. 59, No. 2, 2021, pp. 569–579.

[16] Bogey, C. and Marsden, O., "Influence of nozzle-exit boundary-layer profile on high-subsonic jets," Tech. Rep. 2014-2600, AIAA Paper, 2014.

[17] Bogey, C. and Sabatini, R., "Effects of nozzle-exit boundary-layer profile on the initial shear-layer instability, flow field and noise of subsonic jets," *J. Fluid Mech.*, Vol. 876, 2019, pp. 288–325.

[18] Bogey, C. and Marsden, O., "Numerical investigation of temperature effects on properties of subsonic turbulent jets," Tech. Rep. 2013-2140, AIAA Paper, 2013.

[19] Bogey, C., "A study of the effects of temperature on velocity and density fluctuations in high-subsonic jets," Tech. Rep. 2014-0524, AIAA Paper, 2014.